Scripta Materialia 149 (2018) 11–15

Contents lists available at ScienceDirect

Scripta Materialia

journal homepage: www.elsevier.com/locate/scriptamat

Regular article

Irradiation-induced segregation at phase boundaries in austenitic stainless steel weld metal

Xiaodong Lin [a,b], Qunjia Peng [a,*], En-Hou Han [a], Wei Ke [a], Chen Sun [c], Zhijie Jiao [d]

[a] Key Laboratory of Nuclear Materials and Safety Assessment, Institute of Metal Research, Chinese Academy of Sciences, Shenyang 110016, China
[b] School of Materials Science and Engineering, University of Science and Technology of China, Shenyang 110016, China
[c] State Power Investment Corporation Research Institute, Beijing 102209, China
[d] Department of Nuclear Engineering and Radiological Sciences, University of Michigan, Ann Arbor, MI 48109, USA

ARTICLE INFO

Article history:
Received 24 October 2017
Received in revised form 31 December 2017
Accepted 30 January 2018
Available online xxxx

Keywords:
Austenitic steels
Irradiation
Atom probe tomography
Interface diffusion
Segregation

ABSTRACT

Irradiation-induced segregation (RIS) at phase boundaries in austenitic stainless steel weld metal was studied using atom probe tomography. Irradiation induced depletion of Cr and Mn and enrichment of Ni and Si at the δ-ferrite/austenite, δ-ferrite/carbide and austenite/carbide phase boundaries. The vacancy mechanism and the solute-defect binding model were applied to interpret the RIS at the phase boundaries. The concentration gradients of Cr and Ni at the phase boundary regions reduced Cr depletion but promoted Ni segregation, which caused a difference with the RIS at the grain boundary.

Austenitic stainless steel weld metals consisting of an amount of δ-ferrite phase exhibit enhanced corrosion resistance and have been used as inner surface cladding of reactor pressure vessel (RPV) in light water reactors (LWRs) [1]. The weld metal, however, is subjected to irradiation in the service environment, which induces damage of the microstructure and deteriorates mechanical property [2–4]. Dislocation loops, voids and precipitates were all observed and contributed to the hardening and embrittlement of austenitic stainless steels [5,6]. Irradiation also induces segregation at grain boundaries in austenitic stainless steels, including depletion of Cr and Mn and enrichment of Ni, Si and P [7–11]. Irradiation-induced segregation (RIS) at the grain boundary is attributed to the association of solute atoms with the irradiation-induced point defects [12,13]. While it has been well acknowledged that the grain boundary has a lower resistance to corrosion and cracking [14–16], the segregation could degrade further the property of the grain boundary. For example, segregation of Si and P could lower the boundary bonding strength, leading to embrittlement of the steel [10,17]. Depletion of Cr and enrichment of Si at the grain boundary contributed to intergranular corrosion and cracking in LWR environments [18–20].

Studies on the dual phase weld metal have been only focused on the effect of irradiation on precipitates in the δ-ferrite phase of the steel [6]. Irradiation-induced segregation at the phase boundary has yet to be studied. Particularly, it is not clear whether the different chemical compositions and crystallographic structures on the two sides of the phase boundary may vary the diffusion of solute atoms and cause a different segregation behavior from that at the grain boundary. In this work, RIS at the phase boundaries was investigated using atom probe tomography (APT) in proton-irradiated nuclear grade 308 L austenitic stainless steel weld metal.

The 308 L austenitic stainless steel was extracted from a mockup of the RPV weld cladding. It has a chemical composition of 0.016% C, 0.32% Si, 1.33% Mn, 0.015% P, 19.88% Cr, 10.30% Ni and balance Fe in weight percent. Vermicular δ-ferrite with a size of less than 5 μm was embedded at the dendritic grain boundaries of austenite matrix, shown in Fig. 1(a). Discontinuous precipitate with a size of tens of nanometers existed at the δ-ferrite/austenite phase boundary before irradiation, shown in Fig. 1(b). The precipitate was identified as Cr carbides ($M_{23}C_6$) by the electron diffraction pattern as shown in the inset in Fig. 1(b). Therefore, three kinds of phase boundaries, namely δ-ferrite/austenite (δ/γ), δ-ferrite/carbide (δ/C) and austenite/carbide (γ/C) phase boundaries, were of interest in this study.

Samples for the irradiation experiment had dimensions of 20 × 3 × 2 mm^3. They were ground using emery papers up to 2000 grit and mechanically polished using 2.5 μm and 1 μm diamond pastes to obtain a mirror surface. The irradiation surface (20 × 3 mm^2) was finally polished using a 40 nm colloidal silica slurry to eliminate the surface

* Corresponding author.
E-mail address: pengqunjia@cgnpc.com.cn (Q. Peng).

https://doi.org/10.1016/j.scriptamat.2018.01.033
1359-6462/

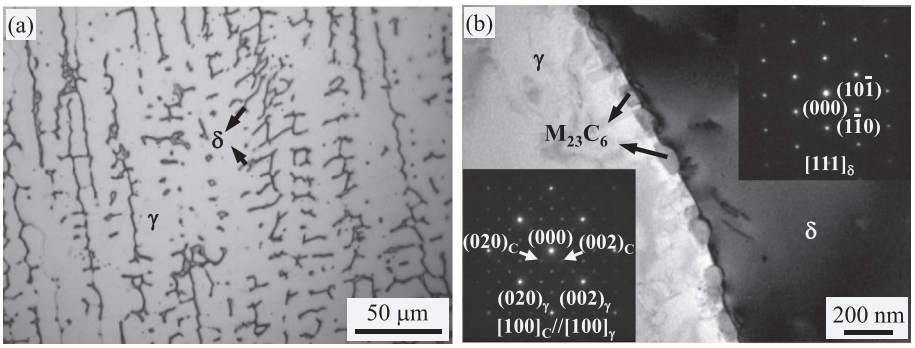

Fig. 1. (a) Metallographic morphology of 308 L stainless steel weld metal showing vermicular δ-ferrite (δ) in austenite (γ) matrix. (b) Transmission electron microscopy image and electron diffraction patterns showing the δ and γ phases as well as the discontinuous Cr carbides ($M_{23}C_6$) at δ/γ phase boundary.

residual strain. Then the surface was irradiated by 2 MeV protons up to 3 displacement per atom (dpa) at 360 °C with a dose rate of 5.96×10^{-6} dpa/s at Michigan Ion Beam Laboratory of the University of Michigan. Details on the irradiation process are available elsewhere [21,22].

Following the proton irradiation, APT tips that contain different phase boundaries were fabricated using a dual-beam focused ion beam instrument (Helios 600i, FEI) using life-out method [23,24]. Tips were examined in an APT system (CAMECA LEAP 4000X HR) using laser pulse mode at 50 K. To prevent the APT tips from fracture during measurements, an optimized laser energy of 60 pJ with a pulse repetition frequency of 200 kHz was used. APT data was analyzed using the IVAS software version 3.6.8. Multiple APT measurements of each type of phase boundary were performed to confirm the repeatability of the measurement (see the Supplementary Material).

Fig. 2(a) through (d) show the results of the APT analysis of the unirradiated and irradiated samples containing a δ/γ phase boundary. Depletion of Cr and Mn and enrichment of Ni, Si and P were observed at the boundary after 3-dpa irradiation, shown in Fig. 2(b). It is notable that a certain degree of the enrichment of Si and P at the phase boundary occurred before irradiation, shown in Fig. 2(a). Composition profiles across the phase boundary before and after irradiation are compared in Fig. 2(c) and (d) for Cr, Ni and Mn, Si, P, respectively. Following irradiation, Cr was depleted to a content of lower than 10 at.% in a region of more than 10 nm wide, while Mn content is as low as 0.2 at.% at the phase boundary. On the other hand, the enrichment of Ni at the phase boundary with a maximum content of about 19 at.% was observed. The irradiation also increased the Si content from 1.1 at.% to 3.7 at.% at the phase boundary. However, the P content at δ/γ phase boundary did not show a certain change after the irradiation, which varied from 0.13 at.% to 0.26 at.% before the irradiation, and from 0.11 at.% to 0.15 at.% after the irradiation (Fig. 2(d) and Fig. S18 in the Supplementary Material). As such, no irradiation effects on the P segregation at δ/γ phase boundary could be confirmed.

Atom maps and concentration profiles across δ/C and γ/C phase boundary regions in the unirradiated and irradiated samples are shown in Fig. 3. Depletion of Cr and Mn and enrichment of Ni, Si and P at both phase boundaries were observed after the 3-dpa irradiation. The Cr-depletion at both phase boundaries showed a minimum content of about 10 at.%, shown in Fig. 3(c). However, the width of the Cr-depleted region at the δ/C phase boundary was approximately two times of that at the γ/C phase boundary. The minimum Mn content in the Mn-depleted regions at δ/C and γ/C phase boundaries was 0.28 at.%

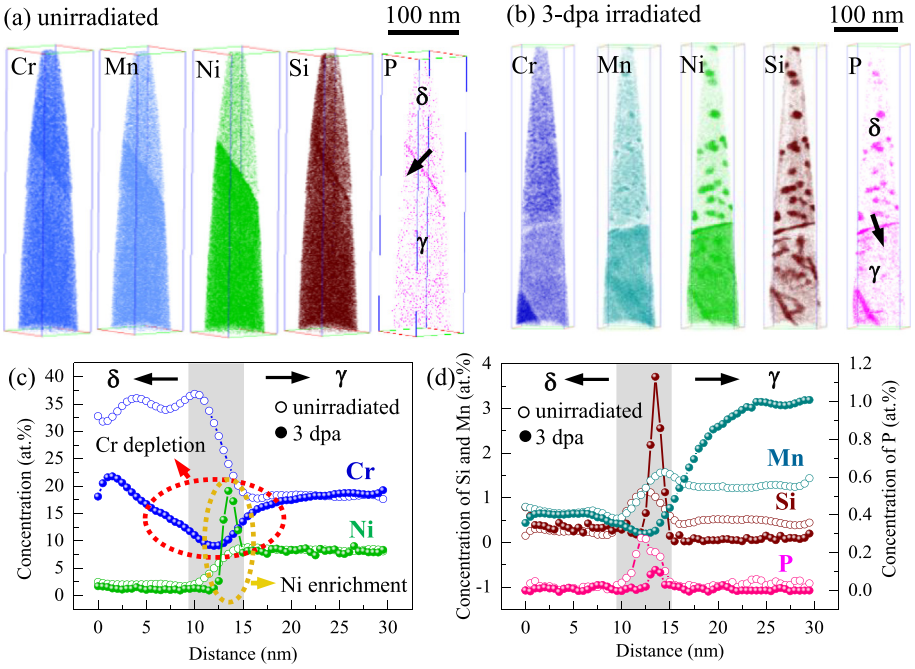

Fig. 2. Atom maps of (a) unirradiated and (b) 3-dpa irradiated samples containing a δ/γ phase boundary (The volume analyzed is $78 \times 78 \times 360$ and $71 \times 71 \times 440$ nm^3, respectively). Effect of irradiation on composition profiles of (c) Cr, Ni and (d) Mn, Si and P across δ/γ phase boundary. The direction of composition profiles across the phase boundary is indicated by the arrows shown in (a) and (b). The grey zone in (c) and (d) indicates the phase boundary region.